JOURNAL OF AIRCRAFT
Vol. 35, No. 4, July–August 1998

Nonlinear Model for Aircraft Brake Squeal Analysis: Stability Analysis and Parametric Studies

James T. Gordon,* Steven Y. Liu,† and M. Akif Özbek‡
The Boeing Company, Seattle, Washington 98124

Results are presented from analyses of primary squeal-mode vibration in aircraft brake systems. System stability is investigated by determining the eigenvalues of linearized perturbation equations at each steady-state operating point of the nonlinear system. Time-history responses are obtained by integrating the complete set of nonlinear dynamic equations. Results are given from analyses conducted using two versions of the nonlinear squeal model, a single-wheel model representing a typical dynamometer configuration, and a fore-aft wheel pair model representing one side of a main landing-gear truck. In general, the model predicts system instability at low braking pressures and stability at high braking pressures. The effects on stability of variations in brake pressure, friction coefficient, and torsional stiffness are shown. The nonlinear squeal model indicates that system instability can occur with a constant friction coefficient and that system stability decreases with increasing brake-friction coefficient. It is shown that proper selection of brake heat stack mechanical properties and design geometry can produce a stable system. Results indicate that a fore-aft brake pair will be more unstable than a single brake, which is in agreement with dynamometer and airplane test data.

Nomenclature

A_p = net piston area, in.^{2}
C_{lug} = lug fore–aft damping coefficient, lb/in./s
C_{wk} = wheel key yaw damping coefficient, lb-in./rad/s
C_{xr} = lateral translational damping coefficient, lb/in./s
C_{xs} = lateral translational damping coefficient, lb/in./s
C_{yax} = axle fore–aft deflection damp coefficient, lb/in./s
C_θ = piston-housing torsional damping coefficient, lb-in./rad/s
$C_{\phi\text{ax}}$ = axle-bending rotation damp coefficient, lb-in./rad/s
$C_{\phi r}$ = yaw viscous damping coefficient, lb-in./rad/s
$C_{\phi s}$ = yaw viscous damping coefficient, lb-in./rad/s
d_e = brake-rod lateral offset, in.
F_{drag} = tire–ground drag load, lb
F_{hyd} = lateral force caused by P_{net}, lb
F_n = lateral contact force, lb
$\hat{F}_n$ = rotor/stator contact stress, lb/in.^{2}
F_{rod} = brake-rod axial load, lb
F_t = tangential force caused by $\hat{F}_n$, lb
$\hat{F}_t$ = tangential stress caused by $\hat{F}_n$, lb/in.^{2}
I_{axle} = axle moment of inertia, lb-in.-s^2
I_θ = stator polar moment of inertia, lb-in.-s^2
$I_{\phi r}$ = yaw polar moment of inertia, lb-in.-s^2
$I_{\phi s}$ = yaw polar moment of inertia, lb-in.-s^2
K_i = coefficients in polynomial for $\hat{F}_n$, (i = 0, 3)
K_{lug} = center lug fore–aft stiffness, lb/in.
K_{rr} = yaw stiffness of rotor, lb-in./rad
K_{wk} = yaw stiffness of wheel key, lb-in./rad
K_θ = piston-housing torsional stiffness, lb-in./rad
$K_{\phi r}$ = rotor yaw stiffness (caused by backing plate), lb-in./rad
$K_{\phi s}$ = stator yaw stiffness, lb-in./rad
K_0 = coefficient of constant term in $\hat{F}_n$, lb/in.^{2}
K_1 = coefficient of linear term in $\hat{F}_n$, lb/in.^{3}
K_2 = coefficient of quadratic term in $\hat{F}_n$, lb/in.^{4}
K_3 = coefficient of cubic term in $\hat{F}_n$, lb/in.^{5}
K_{11} = axle bending $y - y$ stiffness, lb/in.
K_{12} = axle bending $y - \phi$ stiffness, K_{21}, lb/rad
K_{22} = axle bending $\phi - \phi$ stiffness, lb-in./rad
M_b = yaw moment caused by $\hat{F}_n$, lb-in.
m_{axle} = axle mass, lb-s^2/in.
m_{lug} = center-lug mass, lb-s^2/in.
m_r = rotor mass, lb-s^2/in.
m_s = stator mass, lb-s^2/in.
N = number of brake stages, nondimensional
P_{net} = net brake hydraulic pressure, lb/in.^{2}
R_b = piston-housing bushing radius, in.
R_e = distance axle to brake-rod axis, in.
R_i = friction surface inner radius, in.
R_o = friction surface outer radius, in.
R_r = rolling radius of tire, in.
R_w = wheel radius, in.
S = tire slip ratio, nondimensional
T = brake torque, lb-in.
v = aircraft ground speed, in./s
W = aircraft weight per wheel, lb
x_r = rotor lateral displacement, in.
x_s = stator lateral displacement, in.
y_{axle} = axle fore–aft bending, in.
y_{lug} = lug fore–aft deflection, in.
θ_s = piston-housing torsional rotation, rad
μ_{brk} = brake-material friction coefficient, nondimensional
μ_{grd} = ground-friction coefficient, nondimensional
μ_{ph} = piston-housing bushing friction coefficient, nondimensional
μ_r = rotor–wheel key friction coefficient, nondimensional
μ_s = stator–spline friction coefficient, nondimensional
ϕ_{axle} = axle bending rotation, rad
ϕ_r = rotor yaw rotation, rad
ϕ_s = stator yaw rotation, rad
Ω_w = wheel rotation, rad/s

Presented as Paper 96-1252 at the AIAA Dynamics Specialist Conference, Salt Lake City, UT, April 18–19, 1996; received July 29, 1996; revision received Jan. 26, 1998; accepted for publication Jan. 28, 1998.

*Senior Principal Engineer, Structures Vibration Technology. Senior Member AIAA.
†Principal Engineer, Structures Vibration Technology.
‡Senior Specialist Engineer, Structures Vibration Technology. E-mail: akif.ozbek@boeing.com. Member AIAA.

I. Introduction

IN a companion paper, detailed descriptions of a nonlinear model and solution methodology for the analysis of pri-

mary-mode brake squeal in aircraft braking systems are given by Liu et al.[1] The destabilizing mechanism in the model utilizes material surface and volumetric properties of the brake heat stack to couple lateral translation and yaw of the rotors and stators. Geometric and stiffness properties of the brake and landing-gear structure couple piston-housing torsional rotation and axle fore–aft bending with lateral translation and twist of the heat stack.

The model does not require the use of brake-negative damping and predicts that instability can occur with a constant brake-friction coefficient as has been observed during squeal events, particularly with carbon brake systems, on both dynamometer and airplane tests.[1] System stability can be altered by changes in the brake-friction coefficient, pressure, stiffness, geometry, and various brake design parameters. Enhanced versions of the model were presented that include more detailed structural representations of the piston-housing torque tube and the hydraulic flow equations for each piston. The model was extended to a fore–aft wheel pair on a two-axle main landing-gear truck.

In this paper, results are presented from analyses conducted using the nonlinear squeal model and the solution methodology described in a companion paper.[1] The modeling assumptions and solution methodology are reviewed briefly before results are presented.

A. Degrees of Freedom

For a single-wheel model, the degrees of freedom are rigid-body lateral displacement and yaw of the rotor and stator (x_r, ϕ_r and x_s, ϕ_s, respectively); piston-housing rigid-body torsional rotation θ_s; axle fore–aft deflection and bending rotation (y_{axle} and ϕ_{axle}, respectively); and wheel rotation Ω_w.

For the fore–aft wheel pair model, the single-wheel freedoms are included for each wheel plus the fore–aft deflection of the center lug y_{lug} on the landing-gear lower oleo strut.

Additional degrees of freedom required for the brake-hydraulic equations are the piston pressure p_i at each piston, the fluid velocity v_{ij} between two adjacent piston cavities, and the piston-housing axial deflection $x_{i\text{ph}}$ at each piston.

B. Assumptions

The brake-friction coefficient μ_{brk} is assumed to be a constant during a squeal vibration event as suggested by experimental observations. For simplicity, the multistage brake is represented by a single rotor and stator with the effective brake torque T_{eff} being given by $T_{\text{eff}} = 2N\,T_{\text{surf}}$, where T_{surf} is the torque per stage per friction surface. For simplicity, it is assumed that the rotor and stator friction surfaces are always in contact. However, validity of the model is not restricted to these assumptions.

The relative displacement between the rotor and stator is assumed to be a function of rotor and stator rigid-body lateral translation and yaw. The normal contact force at the rotor and stator interface is represented by a cubic polynomial in the relative displacement between the rotor and stator in compression. The nonlinear relationship between load and deflection has been verified by static tests conducted on complete brake heat-stack assemblies and small-scale coupons. Experimental results have shown that the load-deflection relationship is highly nonlinear at low to moderate net-brake pressures (0–500 psi). The nonlinear characteristic is a result of surface irregularities, disk flatness, anisotropic properties of the friction material, etc. As pressure increases, the load-deflection relationship becomes increasingly linear. The heat-stack stiffness clearly is affected by temperature during brake application. However, thermal effects on stability are not addressed in the analyses presented herein.

The brake-rod axial load is assumed to be a function of the piston-housing torsional and yaw rotations plus the axle and center lug fore–aft deflections.

C. Equations of Motion

In a companion paper a detailed description of the nonlinear squeal model and solution methodology is given by Liu et al.[1] The nonlinear squeal equations have the general form

$$[M]\{\ddot{\boldsymbol{x}}\} + [C]\{\dot{\boldsymbol{x}}\} + [K]\{\boldsymbol{x}\} = \{\boldsymbol{F}_{\text{hyd}}\} + \{\boldsymbol{F}_{\text{damp}}\} + \{\boldsymbol{F}_{\text{disk}}\} + \{\boldsymbol{F}_{\text{drag}}\} \tag{1}$$

where dots over a symbol indicate differentiation with respect to time t, and $\{\boldsymbol{x}\}$ is a vector of the time-dependent variables (degrees of freedom)

$$\{\boldsymbol{x}\}^T = \lfloor x_s \;\; \phi_s \;\; \theta_s \;\; x_r \;\; \phi_r \;\; y_{\text{axle}} \;\; \phi_{\text{axle}} \;\; \Omega_w \;\; y_{\text{lug}} \rfloor \tag{2}$$

The components of the matrices and vectors in Eq. (1) are specified in a companion paper.[1]

For a given net-brake hydraulic pressure P_{net} at equilibrium conditions, i.e., smooth sliding, the nonlinear Eq. (1) satisfies the following conditions:

$$[K]\{\boldsymbol{x}_0\} = \{\boldsymbol{F}_{\text{hyd}}\} + \{\boldsymbol{F}_{\text{disk}}(x_0)\} \tag{3}$$

There will be more than one steady-state operating point at a given brake pressure because the squeal equations are nonlinear, and system stability will vary accordingly. In this paper, stability is investigated only about the operating point $\{\boldsymbol{x}_0\}$ attained with a zero starting vector for the Newton–Raphson algorithm[2] used to solve the nonlinear system of equations. This operating point corresponds to the most probable set of equilibrium conditions that the brake system will encounter if the hydraulic pressure is applied gradually.

The linearized squeal equations of motion have the general form

$$[M]\{\ddot{\bar{\boldsymbol{x}}}\} + [C]\{\dot{\bar{\boldsymbol{x}}}\} + [K]\{\bar{\boldsymbol{x}}\} = \{\boldsymbol{F}_{\text{hyd}}\} + \{\boldsymbol{F}_{\text{disk}}(x_0)\} + \{\boldsymbol{F}_{\text{disk}}(\bar{x})\} + \{\boldsymbol{F}_{\text{drag}}(x_0)\} + \{\boldsymbol{F}_{\text{drag}}(\bar{x})\} \tag{4}$$

where $\{\bar{\boldsymbol{x}}\}$ is a vector of small perturbations about the equilibrium point $\{\boldsymbol{x}_0\}$

$$\{\boldsymbol{x}\} = \{\boldsymbol{x}_0\} + \{\bar{\boldsymbol{x}}\} \tag{5}$$

$$\{\bar{\boldsymbol{x}}\}^T = \lfloor \bar{x}_s \;\; \bar{\phi}_s \;\; \bar{\theta}_s \;\; \bar{x}_r \;\; \bar{\phi}_r \;\; \bar{y}_{\text{axle}} \;\; \bar{\phi}_{\text{axle}} \;\; \bar{\Omega}_w \;\; \bar{y}_{\text{lug}} \rfloor \tag{6}$$

Two types of analyses have been conducted. Stability analyses (eigensolution) have been performed on the linearized squeal equations [Eq. (4)] for small perturbations about an operating point of the nonlinear system. In addition, time–history response solutions have been obtained by numerically integrating the nonlinear squeal equations [Eq. (1)] to complement the eigensolution results, evaluate stability of the nonlinear system near the operating points, evaluate stability of limit cycles and strange attractors, and determine response amplitudes, e.g., rod loads, accelerations, etc.

II. Stability Analysis

Stability analyses of the linearized perturbation equations, and time–history response analyses of the complete set of nonlinear squeal equations have identified those model parameters that have the greatest effects on system stability. The major parameters in the nonlinear contact stiffness model that affect system stability are shown as follows: brake heat-stack nonlinear load vs deflection, brake-friction coefficient, brake pressure, piston-housing stator yaw stiffness (axle bushings), torsional stiffness of brake stationary parts, brake-rod lateral offset from axle bushing, wheel key bending stiffness, axle bending stiffness, and ground friction. In this paper only variations in the brake-friction coefficient, brake pressure, and torsional stiffness of the brake stationary parts are discussed in

detail. Nominal parameter values used in all numerical calculations are given in the Appendix.

All stability analyses have been conducted using assumed coefficients for the nonlinear contact stiffness model of $K_0 = K_1 = K_3 = 0$, and $K_2 = 1.0 \times 10^5$ lb/in.^{4}, which represents a strongly nonlinear brake heat-stack load-deflection relationship.

The effect of brake pressure on system stability is shown in Fig. 1, wherein the real part of the most unstable eigenvalue is plotted vs net pressure for the single-wheel model assuming a constant wheel speed $\Omega_w = 120$ rad/s, no tire slip, rigid center lug, i.e., $y_{lug} = \dot{y}_{lug} = 0$, and a brake-friction coefficient $\mu_{brk} = 0.5$. For each pressure value shown in Fig. 1, the operating point was determined from Eq. (3). Stability was investigated by determining the eigensolution of the linearized equations at this equilibrium point.[2] Note that as the pressure increases from 10 to 150 psi, the brake system becomes more unstable and the squeal mode and frequency change, i.e., 203 Hz at 25 psi, 216 Hz at 50 psi, 226 Hz at 75 psi, 233 Hz at 100 psi, and 242 Hz at 150 psi. As the pressure is increased further, the degree of instability is decreased until the system becomes stable above 575 psi net-brake pressure, and the frequency continues increasing to about 500 psi (258 Hz at 300 psi, 264 Hz at 400 psi, and 267 Hz at 500 psi) and then decreases at higher pressures (265 Hz at 550 psi, 258 Hz at 700 psi, and 256 Hz at 800 psi). As the brake pressure is increased beyond 800 psi, the real part of the eigenvalue and the frequency change only slightly, having essentially converged to constant values by 1000-psi net pressure (data are shown only to 1000 psi). From flight-test data, the squeal frequency has been observed to vary over a considerable range as shown in a companion paper,[1] and the nonlinear squeal model clearly exhibits this trait also.

The nonlinear contact stiffness model indicates that system instability can occur with a constant friction coefficient as observed on both dynamometer and airplane tests. In general, stability decreases with increasing brake-friction coefficient. Typically, the system is stable at low values of μ_{brk} and unstable at high values.

Root locus plots are given in Figs. 2 and 3, demonstrating the effect on system stability of a variation in the brake-friction coefficient at two values of brake-net hydraulic pressure, 400 and 800 psi, respectively. For each case, the steady-state operating point of the nonlinear system was determined assuming a brake-friction coefficient of 0.5 and a root locus plot constructed with the brake friction coefficient being the root locus parameter about this nominal condition. As seen in Fig. 2, for a net pressure of 400 psi, the system is marginally stable at a friction coefficient of 0.3 and becomes increasingly unstable as the friction coefficient is increased to values of 0.4 and higher. Figure 3 presents similar data for a net pressure of 800 psi. The increased stability of the system for a net pressure of

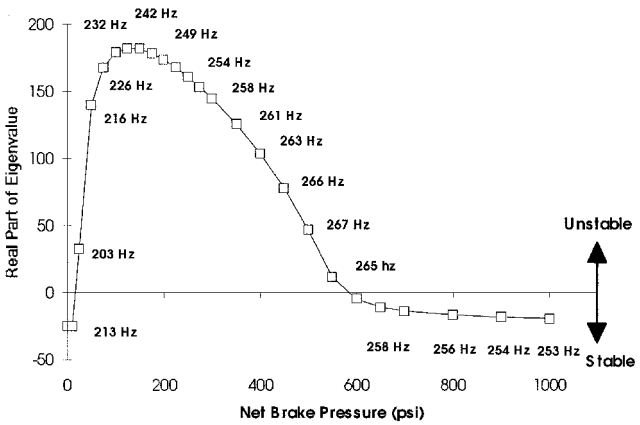

Fig. 1 Pressure effect on system stability.

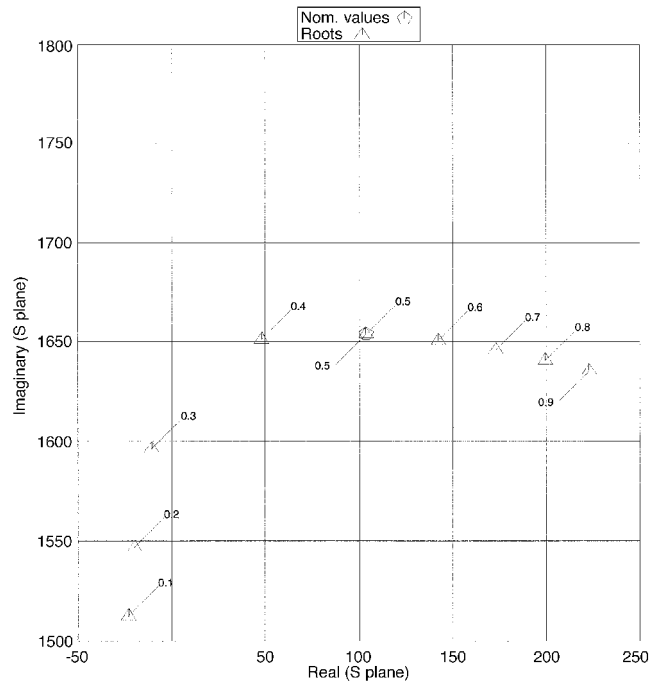

Fig. 2 Brake friction effect on stability, 400 psi.

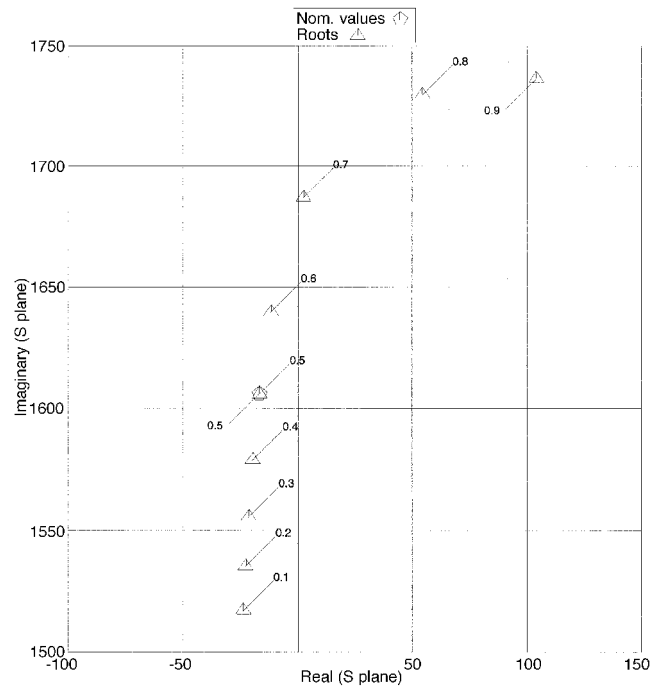

Fig. 3 Brake friction effect on stability, 800 psi.

800 psi is clearly evident because the system is marginally stable at a brake-friction coefficient slightly less than 0.7.

The effect of a variation in torsional stiffness K_θ (as a result of the brake-rod's axial stiffness and the effective fore–aft stiffnesses of the brake torque arm and connecting pins) is shown in Fig. 4 for a net-brake pressure of 200 psi and a brake-friction coefficient of 0.7. Only roots for the unstable squeal mode and two nearby stable modes are shown. Note that as the torsional stiffness is increased above its nominal value of 50×10^6 lb-in./rad, the squeal mode becomes increasingly unstable. As the torsional stiffness is decreased from its nominal value, the system becomes less unstable until it is neutrally stable at a value of about 20×10^6 lb-in./rad and marginally stable at a value of 10×10^6 lb-in./rad. However,

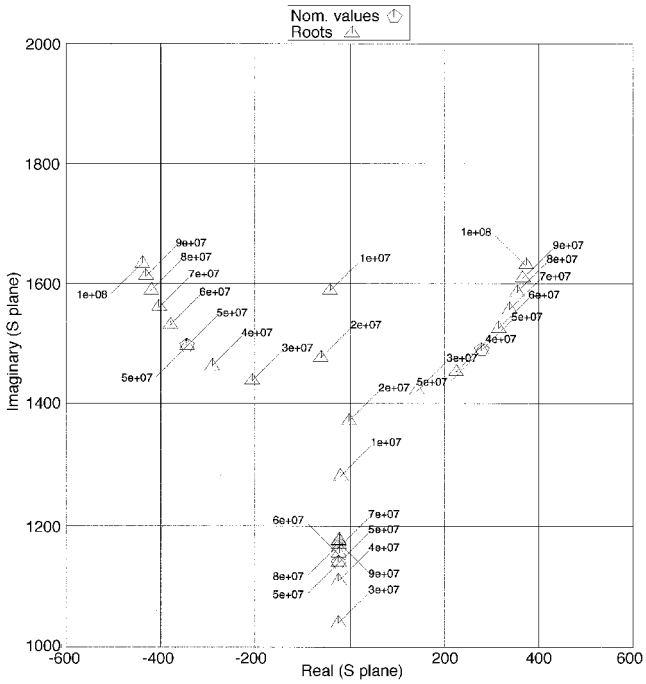

Fig. 4 Torsional stiffness effect on stability.

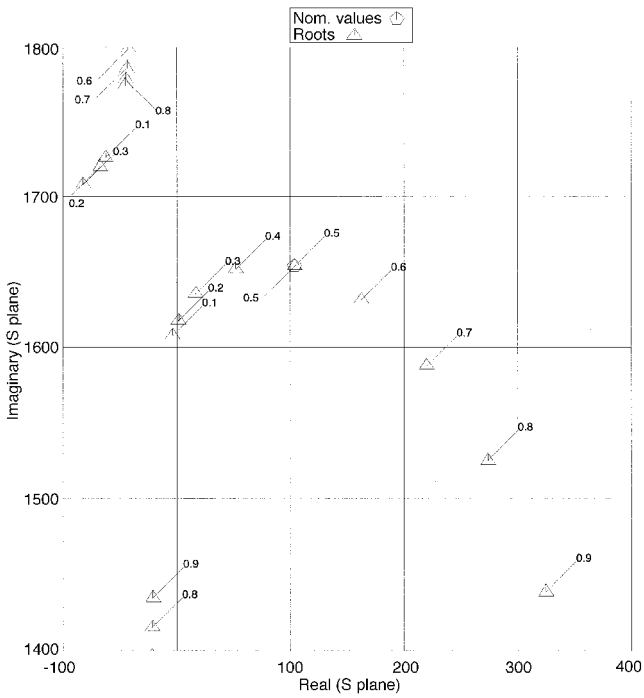

Fig. 5 Friction effect on fore–aft pair stability, 400 psi.

this is a fivefold decrease in stiffness that would not be acceptable in practice because this structure is sized for strength.

Figure 5 presents a root locus plot that demonstrates the effect on stability of a variation in the brake-friction coefficient for the fore–aft pair model at 400-psi net-hydraulic pressure. The plot was constructed by determining the steady-state operating point of the nonlinear system assuming a friction coefficient of 0.5 on the forward brake with the friction coefficient of the aft brake being the root locus parameter. As shown in Fig. 2 for the single-wheel model at a net pressure of 400 psi, the brake system is marginally stable at a friction coefficient of about 0.33 and becomes increasingly unstable as the friction coefficient is increased further. As shown in Fig. 5 for the fore–aft pair model, the system becomes unstable for an aft-brake friction coefficient of about 0.20 demonstrating the decreased stability of the fore–aft brake pair compared with that of the single-wheel model.

III. Transient Response Analysis

Time–history response solutions have been obtained using a variable-step fourth-order Runge–Kutta algorithm[2] to integrate the nonlinear squeal equations [Eq. (1)] for both the single-wheel and fore-aft wheel pair models assuming a constant wheel speed $\Omega_w = 120$ rad/s and no tire slip. Coulomb friction formulations were used to model damping for the piston-housing bushing, rotor-wheel key, and stator spline. The single-wheel model is representative of a typical dynamometer configuration. The fore–aft wheel pair model is representative of one side of an airplane main-landing truck. A maximum time step of 1.0×10^{-5} s was used in these calculations.

All transient response analyses were conducted using coefficients for the nonlinear contact stiffness model obtained from a least-squares fit to load-deflection data taken from a typical brake heat stack, where $K_0 = 0$; $K_1 = 17{,}542$ lb/in.[3]; $K_2 = -2.7141 \times 10^6$ lb/in.[4]; and $K_3 = 105.43 \times 10^6$ lb/in.[5]. With these coefficients, the load-deflection cubic polynomial is valid only for a net-heat stack compression of 0.14 in., i.e., 28-psi net pressure, or greater. This corresponds to heat-stack lateral deflections of approximately $x_s(1) = x_s(2) = 0.015$ in. and $x_r(1) = x_r(2) = 0.001$ in. All response calculations used initial conditions corresponding to the steady-state state operating point associated with a net-brake hydraulic pressure of 28 psi. A transient pulse ΔT, consisting of a one-cycle, 200-Hz cosine perturbation to the brake torque T, was applied to the system at time $t = 0.1$ s to investigate system stability.

Figure 6 shows the predicted brake-rod axial load response F_{rod} to a pressure-ramp input for the single-wheel model with initial conditions for 28-psi net pressure and nominal parameter values. The pressure ramp P_{net} rises to a constant level of 360 psi at time $t = 0.05$ s (the total hydraulic load F_{hyd} is shown in the plot). For this analysis, a nominal center lug stiffness $K_{\text{lug}} = 1.63 \times 10^6$ lb/in. was assumed. A Coulomb friction coefficient of 0.10, which is a typical value for well-lubricated surfaces, was assumed for the rotor–wheel key, stator spline, and piston-housing bushing. A brake-friction coefficient of 0.45 was assumed; this is a typical value during a high-speed taxi or landing rollout braking-squeal event for a carbon brake. At time $t = 0.1$ s, a one-cycle torque perturbation ΔT_1 of mag-

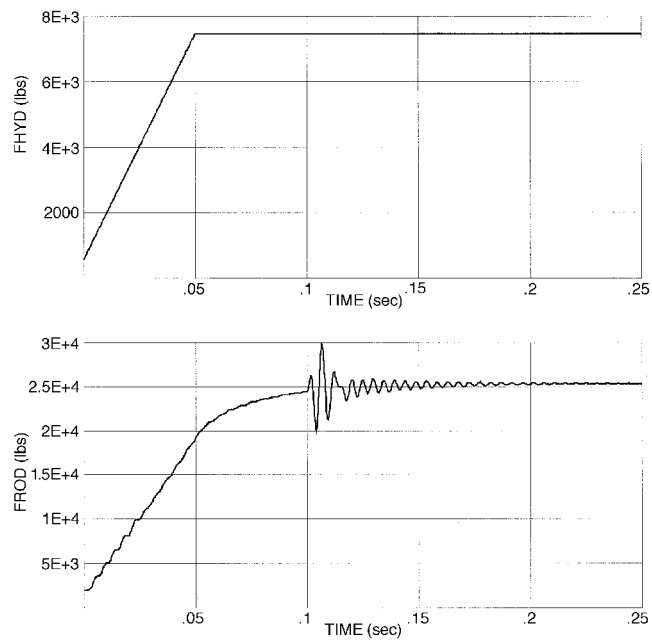

Fig. 6 Single-wheel response, $\mu = 0.45$, ΔT_1.

nitude 28,200 lb-in. (which corresponds to a rod load of 3000 lb), was applied for 0.005 s (200 Hz). As seen in the plot, the brake-rod load has a dynamic component that is excited after the torque pulse is applied, reaching a maximum of approximately 30 kips, and quickly decaying to the steady-state level of about 25 kips.

Figure 7 shows the predicted brake-rod axial load response F_{rod} for the single-wheel model subjected to the same pressure ramp input, initial conditions, torque pulse ΔT_1, and nominal parameter values used for Fig. 6, but with a slightly higher brake-friction coefficient $\mu_{brk} = 0.50$ being assumed. The response is similar to that obtained with a friction coefficient of 0.45 but the amplitudes are slightly higher for the peak (32.5 kips), dynamic, and steady-state (28.2 kips) rod-load components.

For the single-wheel model with a rigid center lug, a brake-friction coefficient of 0.50, torque pulse ΔT_1, and all other parameter values identical to those used to produce Figs. 6 and 7, the response (not shown here) is similar to that in Fig. 7, except that in this case the peak load is about 34.3 kips.

Figure 8 shows the predicted brake-rod axial load responses in the forward rod $F_{rod}(1)$, and in the aft rod $F_{rod}(2)$, for the fore–aft wheel pair model subjected to the same pressure ramp input, initial conditions, and nominal parameter values used for the single-wheel analysis just discussed. A torque pulse ΔT_1 of $-28{,}200$ lb-in. was applied to the forward brake, and a pulse of $+28{,}200$ lb-in. was applied to the aft brake at time $t = 0.1$ s. Different signs were selected for the torque pulses on the fore and aft brakes merely to excite the out-of-phase squeal mode (based on rod-load response) more quickly than if the same sign was assumed for each pulse. For this analysis, the nominal center-lug stiffness was included. Coulomb-friction coefficients for the rotor–wheel key, stator spline, and piston-housing bushing were assumed to be 0.10. A brake-friction coefficient of 0.50 was assumed on both the forward and aft brakes. As seen in Fig. 8, the brake-rod load responses are similar to that of the single-wheel model, shown in Figs. 6 and 7, and reach a maximum of approximately 33 kips on the forward rod and about 34 kips on the aft rod.

Figure 9 shows the effect on predicted brake-rod axial load response of a change in the magnitude of the torque pulse applied to the single-wheel model. A one-cycle, 200-Hz torque pulse $\Delta T_2 = 40{,}000$ lb-in. (rod load of 4255 lb) was applied at time $t = 0.1$ s. A brake coefficient of 0.50 was assumed on the brake. All other model parameters had the same nominal values, pressure ramp, and initial conditions used to produce Fig. 7. The response is similar to that shown in Fig. 7 for the same brake-friction coefficient of 0.50 with a lower amplitude torque pulse $\Delta T_1 = 28{,}200$ lb-in. As shown in Fig. 9, the system is stable and the rod-load response peak amplitude is slightly higher (36.3 kips) than that for the lower-amplitude torque pulse $\Delta T_1 = 28{,}200$ lb-in.

Figure 10 presents brake-rod load responses and total pressure loads of the fore and aft rods when the fore–aft model is subjected to a higher amplitude torque pulse $\Delta T_2 = 40{,}000$ lb-in. at time $t = 0.1$ s than was used to produce the results in Fig. 8. As can be seen by comparing Figs. 9 and 10, response of the fore–aft pair model now is quite different, both qualitatively and quantitatively, from responses of either the single-wheel model with the same torque pulse $\Delta T_2 = 40{,}000$ lb-in., or the fore–aft pair model with a lower level torque pulse ΔT_1

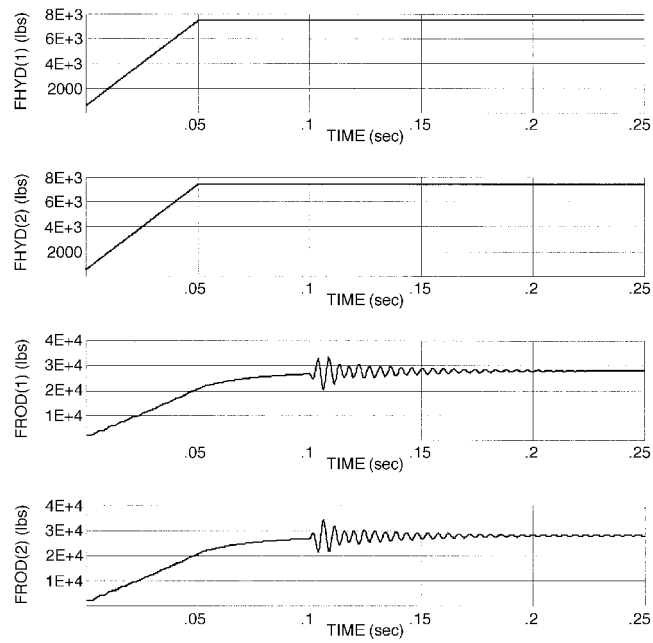

Fig. 8 Fore–aft response, ΔT_1, $\mu = 0.50/0.50$.

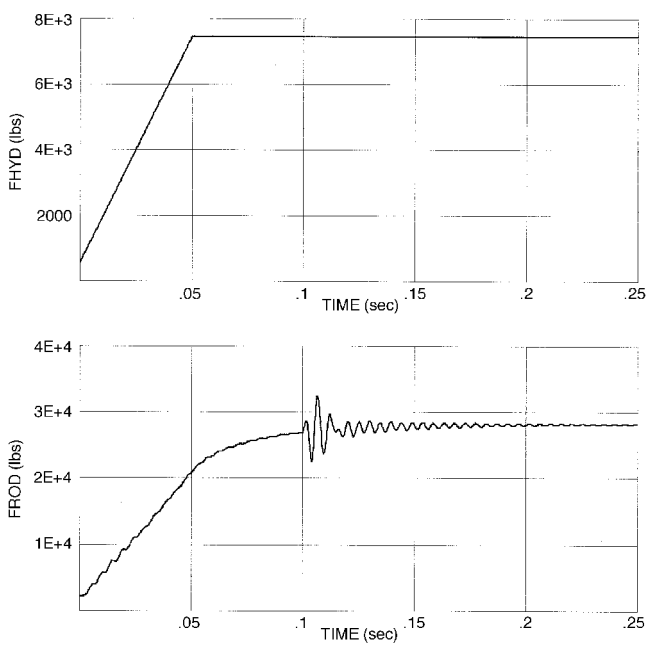

Fig. 7 Single-wheel response, $\mu = 0.50$, ΔT_1.

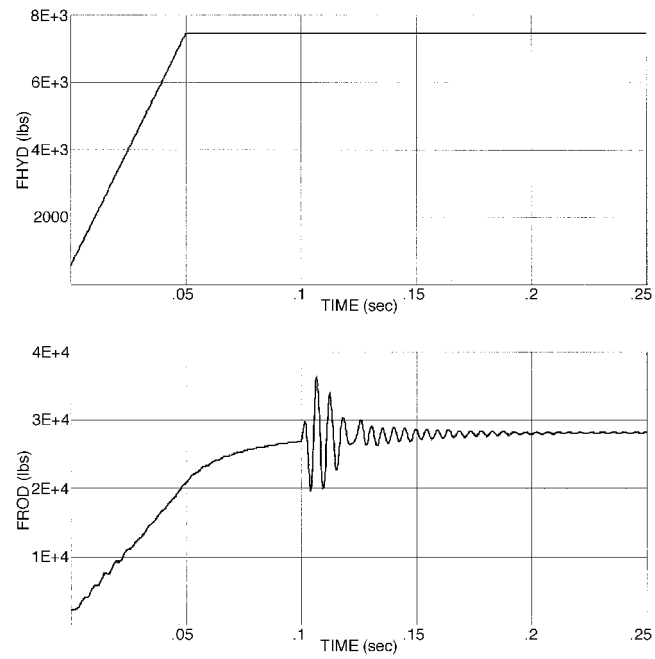

Fig. 9 Single-wheel response, ΔT_2, $\mu = 0.50$.

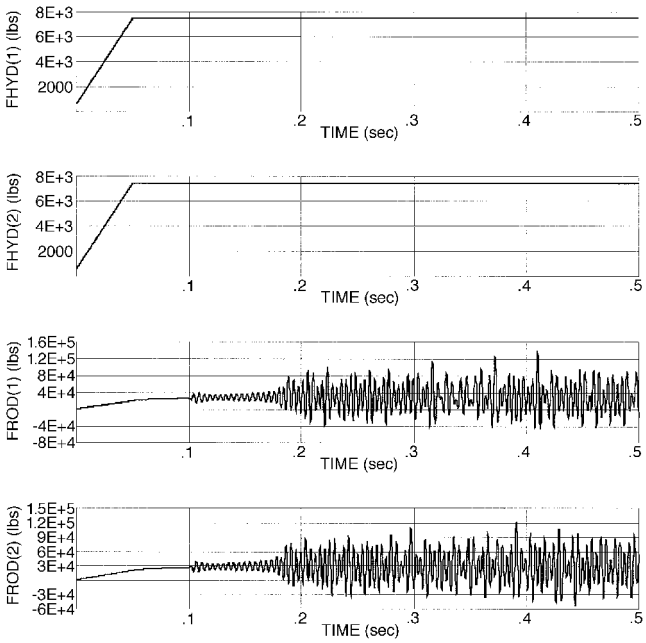

Fig. 10 Fore–aft response, ΔT_2, μ = 0.50/0.50.

= 28,200 lb-in. For the same torque pulse ΔT_2, the single-wheel model is stable. For the fore–aft pair model, the higher-amplitude torque pulse ΔT_2 has excited a high-amplitude limit cycle response with the brake-rod loads reaching maximums of approximately 138 and 122 kips on the forward and aft rods, respectively.

These results indicate that a fore–aft brake pair will be more unstable than a single brake, which is in agreement with dynamometer and airplane test data. Also, the aft-brake-rod loads are generally, but not always, somewhat higher than the forward rod loads for similar friction coefficient values, as can be seen in Figs. 8 and 10. Depending on initial conditions and operating point stability, limit-cycle oscillations may or may not be obtained.

IV. Summary and Conclusions

Results were presented from analyses of primary squeal-mode vibration in aircraft brake systems using two versions of a nonlinear squeal model. One version, representing a typical dynamometer configuration, included a single brake, wheel, brake rod, and cantilevered axle. The second version, representing one side of a main-landing-gear truck, included a fore–aft pair of brakes and wheels connected by two brake rods to the lower oleo center lug. In these analyses, the contact stress between the brake rotor and stator was represented by a cubic polynomial in the relative displacement normal to the friction surface.

The destabilizing mechanism in the model utilized mechanical and material surface properties of the brake heat stack to couple lateral translation and yaw of the rotors and stators. Geometric and stiffness properties of the brake and landing-gear structure coupled torsional rotation of the brake stationary parts and axle fore–aft bending with lateral translation and twist of the heat stack. The nonlinear equations of motion were linearized about the steady-state operating point and a set of linearized perturbation equations was obtained. Stability was investigated by determining eigenvalues of the linearized perturbation equations about each operating point. The complete set of nonlinear dynamic equations was integrated numerically to obtain time–history responses.

In general, the nonlinear contact stiffness model predicted system instability at low braking pressures and stability at high braking pressures. The effects on system stability of changes in brake-friction coefficient, pressure, and torsional stiffness were investigated. System stability decreased with increasing brake-friction coefficient. Typically, the system was stable at low values of the brake-friction coefficient and unstable at high values. It was shown that proper selection of brake heat-stack mechanical properties and design geometry can produce a stable system. Results indicated that a fore–aft brake pair will be more unstable than a single brake, which is in agreement with dynamometer and flight-test data.

Appendix: Nominal Parameter Values

Ω_w = 120 rad/s
A_p = 20.7 in.^{2}
$C_{\phi r}$ = 200 lb-in./rad/s (100 in Fig. 4, 300 in Figs. 6–10)
$C_{\phi s}$ = 200 lb-in./rad/s (100 in Fig. 4, 300 in Figs. 6–10)
C_{xr} = 10 lb/in./s (Figs. 1–3, 5), 100 lb/in./s (Fig. 4), 0 lb/in./s (Figs. 6–10)
C_{xs} = 10 lb/in./s (Figs. 1–3, 5), 100 lb/in./s (Fig. 4), 0 lb/in./s (Figs. 6–10)
C_{wk} = 125 lb-in./rad/s (100 in Fig. 4, 200 in Figs. 6–10)
C_θ = 0 (1400 lb-in./rad/s in Figs. 1–5)
d_e = 1.8 in.
$I_{\phi s}$ = 5.52 lb-in.-s^2
$I_{\phi r}$ = 7.3 lb-in.-s^2
I_θ = 24.67 lb-in.-s^2
K_{11} = 6.71818 $\times$ 10^6 lb/in.
K_{12} = $-$3.19114 $\times$ 10^7 lb/rad = K_{21}
K_{22} = 2.02105 $\times$ 10^8 lb-in./rad
K_0 = 0 lb/in.^{2} (Figs. 1–10)
K_1 = 0 lb/in.^{3} (Figs. 1–5); 17,542.0 (Figs. 6–10)
K_2 = 1.0 $\times$ 10^5 lb/in.^{4} (Figs. 1–5); $-$2.7141 $\times$ 10^6 lb/in.^{4} (Figs. 6–10)
K_3 = 0 lb/in.^{5} (Figs. 1–5), 105.43 $\times$ 10^6 (Figs. 6–10)
K_θ = 50.0 $\times$ 10^6 lb-in./rad
K_{rr} = 2.0 $\times$ 10^6 lb-in./rad
K_{wk} = 2.0 $\times$ 10^6 lb-in./rad
$K_{\phi r}$ = 7.0 $\times$ 10^6 lb-in./rad
$K_{\phi s}$ = 12.0 $\times$ 10^6 lb-in./rad
N = 5
m_s = 0.114 lb-s^2/in.
m_r = 0.128 lb-s^2/in.
μ_s = 0.10 (Figs. 6–10), 0 (Figs. 1–5)
μ_r = 0.10 (Figs. 6–10), 0 (Figs. 1–5)
μ_{ph} = 0.10 (Figs. 6–10), 0 (Figs. 1–5)
R_e = 9.4 in.
R_b = 2.75 in.
R_i = 5.5 in.
R_o = 8.47 in.
C_{lug} = 35.7 lb/in./s
$C_{\phi ax}$ = 20 lb-in./rad/s (100 in Figs. 6–10)
C_{yax} = 20 lb/in./s (100 in Figs. 6–10)
I_{axle} = 16.0 lb-in.-s^2
K_{lug} = 1.63 $\times$ 10^6 lb/in.
m_{axle} = 1.097 lb-s^2/in.
m_{lug} = 0.049 lb-s^2/in.
μ_{grd} = 0.3
R_w = 8.75 in.
R_r = 22.0 in.
S = 0 (no slip)
W = 30,000 lb
v = 2640 in./s

Acknowledgment

The authors would like to thank J. L. Kanning of The Boeing Company for his careful technical review of this paper, helpful comments, and suggestions.

References

[1]Liu, S. Y., Gordon, J. T., and Özbek, M. A., "Nonlinear Model for Aircraft Brake-Squeal Analysis: Model Description and Solution Methodology," *Journal of Aircraft*, Vol. 35, No. 4, 1998, pp. 623–630.

[2]*Easy5x Users Guide*, Boeing Computer Services Document BCS 20491-0530-R1, The Boeing Co., Seattle, WA, Jan. 1993.